Nonlinear propagation in silicon-based plasmonic waveguides from the standpoint of applications

Ivan D. Rukhlenko,[1,*] **Malin Premaratne,**[1] **and Govind P. Agrawal**[2]

[1]*Advanced Computing and Simulation Laboratory (AχL), Department of Electrical and Computer Systems Engineering, Monash University, Clayton, VIC 3800, Australia*
[2]*Institute of Optics, University of Rochester, Rochester, NY 14627, USA*
[*]*ivan.rukhlenko@monash.edu*

Abstract: Silicon-based plasmonic waveguides can be used to simultaneously transmit electrical signals and guide optical energy with deep subwavelength localization, thus providing us with a well needed connecting link between contemporary nanoelectronics and silicon photonics. In this paper, we examine the possibility of employing the large third-order nonlinearity of silicon to create active and passive photonic devices with silicon-based plasmonic waveguides. We unambiguously demonstrate that the relatively weak dependance of the Kerr effect, two-photon absorption (TPA), and stimulated Raman scattering on optical intensity, prevents them from being useful in μm-long plasmonic waveguides. On the other hand, the TPA-initiated free-carrier effects of absorption and dispersion are much more vigorous, and have strong potential for a variety of practical applications. Our work aims to guide research efforts towards the most promising nonlinear optical phenomena in the thriving new field of silicon-based plasmonics.

OCIS codes: (040.6040) Silicon; (190.4390) Nonlinear optics, integrated optics; (240.6680) Surface plasmons; (250.5403) Plasmonics; (130.0250) Optoelectronics.

References and links

1. G. T. Reed and A. P. Knights, *Silicon Photonics: An Introduction* (Wiley, Hoboken, 2004).
2. B. Jalali, O. Boyraz, V. Raghunathan, D. Dimitropoulos, and P. Koonath, "Silicon Raman amplifiers, lasers and their applications," in *Active and Passive Optical Components for WDM Communications V*, A. K. Dutta, Y. Ohishi, N. K. Dutta, and J. Moerk, Eds., Proc. SPIE **6014**, 21–26 (2005).
3. H. Rong, R. Jones, A. Liu, O. Cohen, D. Hak, A. Fang, and M. Pannicia, "A continuous-wave Raman silicon laser," Nature **433**, 725–728 (2005).
4. R. Jones, A. Liu, H. Rong, M. Paniccia, O. Cohen, and D. Hak, "Lossless optical modulation in a silicon waveguide using stimulated Raman scattering," Opt. Express **13**, 1716–1723 (2005).
5. T. K. Liang, L. R. Nunes, M. Tsuchiya, K. S. Abedin, T. Miyazaki, D. V. Thourhout, W. Bogaerts, P. Dumon, R. Baets, and H. Tsang, "High speed logic gate using two-photon absorption in silicon waveguides," Opt. Commun. **265**, 171–174 (2006).
6. B. Jalali, V. Raghunathan, D. Dimitropoulos, and O. Boyraz, "Raman-based silicon photonics," IEEE J. Sel. Top. Quantum Electron. 12, 412–421 (2006).
7. R. A. Soref, "The past, present, and future of silicon photonics," IEEE J. Sel. Top. Quantum Electron. **12**, 1678–1687 (2006).
8. R. Dekker, A. Driessen, T. Wahlbrink, C. Moormann, J. Niehusmann, and M. Först, "Ultrafast Kerr-induced all-optical wavelength conversion in silicon waveguides using 1.55 μm femtosecond pulses," Opt. Express **14**, 8336–8346 (2006).

#136997 - $15.00 USD Received 21 Oct 2010; revised 13 Dec 2010; accepted 17 Dec 2010; published 22 Dec 2010

9. J. Y. Lee, L. Yin, G. P. Agrawal, and P. M. Fauchet, "Ultrafast optical switching based on nonlinear polarization rotation in silicon waveguides," Opt. Express **18**, 11514–11523 (2010).
10. L. Tang, S. Latif, and D. A. B. Miller, "Plasmonic device in silicon CMOS," Electron. Lett. **45**, 706 (2009).
11. J. A. Dionne, L. A. Sweatlock, M. T. Sheldon, A. P. Alivisatos, and H. A. Atwater, "Silicon-based plasmonics for on-chip photonics," IEEE J. Sel. Top. Quantum Electron. **16**, 295–306 (2010).
12. S. M. Sederberg, V. Van, and A. Y. Elezzabi, "Silicon-based plasmonic waveguides interfaced to silicon photonic platform," in Quantum Electronics and Laser Science Conference, OSA Technical Digest (CD) (Optical Society of America, 2010), paper JThE4.
13. J. N. Caspers, N. Rotenberg, and H. M. van Driel, "Ultrafast silicon-based active plasmonics at telecom wavelengths," Opt. Express **18**, 19761–19769 (2010).
14. J. A. Schuller, E. S. Barnard, W. Cai, Y. C. Jun, J. S. White, and M. L. Brongersma, "Plasmonics for extreme light concentration and manipulation," Nature Mater. **9**, 193–204 (2010).
15. M. L. Brongersma, R. Zia, and J. A. Schuller, "Plasmonics—the missing link between nanoelectronics and microphotonics," Appl. Phys. A **89**, 221–223 (2007).
16. S. A. Maier, *Plasmonics: Fundamentals and Applications*, (Springer, 2007).
17. E. Ozbay, "Plasmonics: Merging photonics and electronics at nanoscale dimensions," Science **311**, 189–193 (2006).
18. W. L. Barnes, A. Dereux, and T. W. Ebbesen, "Surface plasmon subwavelength optics," Nature **424**, 824–830 (2003).
19. J. M. Pitarke, V. M. Silkin, E. V. Chulkov, and P. M. Echenique, "Theory of surface plasmons and surface-plasmon polaritons," Rep. Prog. Phys. **70**, 1–87 (2007).
20. U. Schröter and A. Dereux , "Surface plasmon polaritons on metal cylinders with dielectric core," Phys. Rev. B **64**, 125420(1–10) (2001).
21. M. A. Noginov, V. A. Podolskiy, G. Zhu, M. Mayy, M. Bahoura, J. A. Adegoke, B. A. Ritzo, and K. Reynolds, "Compensation of loss in propagating surface plasmon polariton by gain in adjacent dielectric medium," Opt. Express **16**, 1385–1392 (2008).
22. S. A. Maier, "Gain-assisted propagation of electromagnetic energy in subwavelength surface plasmon polariton gap waveguides," Opt. Commun. **258**, 295–299 (2006).
23. M. P. Nezhad, K. Tetz, and Y. Fainman, "Gain assisted propagation of surface plasmon polaritons on planar metallic waveguides," Opt. Express **12**, 4072–4079 (2004).
24. M. Makarova, Y. Gong, S.-L. Cheng, Y. Nishi, S. Yerci, R. Li, L. D. Negro, and J. Vučović, "Photonic crystal and plasmonic silicon-based light sources," IEEE J. Sel. Top. Quantum Electron. **16**, 132–140 (2010).
25. A. Hryciw, Y. C. Jun, and M. L. Brongersma, "Plasmonics: Electrifying plasmonics on silicon," Nature Mater. **9**, 3–4 (2010).
26. R. J. Walters, R. V. A. van Loon, I. Brunets, J. Schmitz, and A. Polman, "A silicon-based electrical source of surface plasmon polaritons," Nature Mater. **9**, 21–25 (2010).
27. A. V. Krasavin and A. V. Zayats, "Silicon-based plasmonic waveguides," Opt. Express **18**, 11791–11799 (2010).
28. B. A. Daniel and G. P. Agrawal, "Vectorial nonlinear propagation in silicon nanowire waveguides: Polarization effects," J. Opt. Soc. Am. B **27**, 956–965 (2010).
29. S. Afshar and T. M. Monro, "A full vectorial model for pulse propagation in emerging waveguides with subwavelength structures part I: Kerr nonlinearity," Opt. Express **17**, 2298–2318 (2009).
30. X. Chen, N. C. Panoiu, and R. M. Osgood, Jr., "Theory of Raman-mediated pulsed amplification in silicon-wire waveguides," IEEE J. Quantum Electron. **42**, 160–170 (2006).
31. J. Bures, *Guided Optics: Optical Fibers and All-fiber Components* (Wiley-VCH, Weinheim, 2009).
32. J. A. Dionne, L. A. Sweatlock, H. A. Atwater, and A. Polman, "Plasmon slot waveguides: Towards chip-scale propagation with subwavelength-scale localization," Phys. Rev. B **73**, 035407(1–9) (2006).
33. A. W. Snyder and J. D. Love, *Optical Waveguide Theory* (Chapman and Hall, London, 1983).
34. I. D. Rukhlenko, M. Premaratne, and G. P. Agrawal, "Nonlinear silicon photonics: Analytical tools," IEEE J. Sel. Top. Quantum Electron. **16**, 200–215 (2010).
35. H. K. Tsang and Y. Liu, "Nonlinear optical properties of silicon waveguides," Semicond. Sci. Technol. **23**, 064007(1–9) (2008).
36. M. Dinu, F. Quochi, and H. Garcia, "Third-order nonlinearities in silicon at telecom wavelengths," Appl. Phys. Lett. **82**, 2954–2956 (2003).
37. C. M. Dissanayake, M. Premaratne, I. D. Rukhlenko, and G. P. Agrawal, "FDTD modeling of anisotropic nonlinear optical phenomena in silicon waveguides," Opt. Express **18**, 21427–21448 (2010).
38. I. D. Rukhlenko, M. Premaratne, C. Dissanayake, and G. P. Agrawal, "Nonlinear pulse evolution in silicon waveguides: An approximate analytic approach," J. Lightwave Technol. **27**, 3241–3248 (2009).
39. Q. Lin, O. J. Painter, and G. P. Agrawal, "Nonlinear optical phenomena in silicon waveguides: Modeling and applications," Opt. Express **15**, 16604–16644 (2007).
40. A. Pannipitiya, I. D. Rukhlenko, M. Premaratne, H. T. Hattori, and G. P. Agrawal, "Improved transmission model for metal-dielectric-metal plasmonic waveguides with stub structure," Opt. Express **18**, 6191–6204 (2010).
41. I. D. Rukhlenko, M. Premaratne, and G. P. Agrawal, "Analytical study of optical bistability in silicon ring res-

#136997 - $15.00 USD Received 21 Oct 2010; revised 13 Dec 2010; accepted 17 Dec 2010; published 22 Dec 2010

onators," Opt. Lett. **35**, 55–57 (2010).
42. Q. Xu and M. Lipson, "Carrier-induced optical bistability in silicon ring resonators," Opt. Lett. **31**, 341–343 (2006).
43. Q. Xu and M. Lipson, "All-optical logic based on silicon micro-ring resonators," Opt. Express **15**, 924–929 (2007).
44. I. D. Rukhlenko, M. Premaratne, and G. P. Agrawal, "Analytical study of optical bistability in silicon-waveguide resonators," Opt. Express **17**, 22124–22137 (2009).
45. M. W. Geis, S. J. Spector, R. C. Williamson, and T. M. Lyszczarz, "Submicrosecond, submilliwatt, silicon-on-insulator thermooptic switch," IEEE Photon. Technol. Lett. **16**, 2514–2516 (2004).
46. S. Abdollahi and M. K. Moravvej-Farshi, "Effects of heat induced by two-photon absorption and free-carrier absorption in silicon-on-insulator nanowaveguides operating as all-optical wavelength converters," Appl. Opt. **48**, 2505–2514 (2009).
47. D. F. Logan, P. E. Jessop, A. P. Knights, G. Wojcik, and A. Goebel, "Optical modulation in silicon waveguides via charge state control of deep levels," Opt. Express **17**, 18571–18580 (2009).
48. J. Basak, L. Liao, A. Liu, D. Rubin, Y. Chetrit, H. Nguyen, D. Samara-Rubio, R. Cohen, N. Izhaky, and M. Paniccia, "Developments in gigascale silicon optical modulators using free carrier dispersion mechanisms," Adv. Opt. Technol. **2008**, 678948(1–10) (2008).
49. E. K. Tien, F. Qian, N. S. Yuksek, and O. Boyraz, "Influence of nonlinear loss competition on pulse compression and nonlinear optics in silicon," Appl. Phys. Lett. **91**, 201115(1–3) (2007).

1. Introduction

Silicon is beginning to be considered for on-chip integration of recently demonstrated photonic devices [1–9] with mainstream electronic components [10–13]. Such an integration will eliminate the basic drawbacks of electronic circuitry and become a significant milestone in the development of power-efficient, high-speed optical supercomputers. One of the major obstacles we face when trying to bring photonics functionalities to the scale of nanoelectronics is the diffraction of light. Specifically, the diffraction phenomenon places a fundamental limit on the miniaturization of photonic devices fabricated with silicon-on-insulator (SOI) technology. Even the smallest SOI waveguides have dimensions of ~ 300 nm [1, 6, 7], which are about ten times what is required for successful integration of electronics and photonics for novel breakthrough applications.

Assistance in the controlling of light on the nanoscale comes from the paradigm of plasmonics [14–18]. In certain situations, light can interact with collective oscillation of electron-hole plasma and form coupled waves known as surface plasmon polaritons (SPPs) [19, 20]. The metal–semiconductor nanowires that guide SPPs are not restricted by the diffraction limit of light and are suitable for carrying information at bit rates comparable to that of high-bandwidth fiber-optic channels. A marriage of silicon photonics with plasmonics will merge the advantages of optical data transfer with the strongest points of modern nanotechnology, facilitating the development of all-optical chips for future supercomputers.

Before such supercomputers can be realized on a silicon platform, a number of technical issues need to be solved and fundamental questions answered. Many of these issues have recently been investigated, and continue to receive much attention [11–13]. Among them is the problem of strong dissipation of SPPs which normally decay within a distance of a few tens of micrometers [21–23]. Another challenge is to create a CMOS-compatible source of SPPs that would allow their generation through electrical pumping [24–26]. Of primary importance are also the questions of the coupling efficiency of closely spaced nanowires, and their interaction with the environment [27]. In this paper, we address a further important question that naturally arises in connection with the adoption of silicon-based functionalities by plasmonic nanowires, which is whether or not the nonlinear effects in silicon are strong enough to control the propagation of SPPs along silicon–metal nanowaveguides. This is a nontrivial issue, as deep subwavelength localization of an optical field makes the nonlinear effects more pronounced, but the short lifetime of SPPs severely limits the interaction length.

#136997 - $15.00 USD Received 21 Oct 2010; revised 13 Dec 2010; accepted 17 Dec 2010; published 22 Dec 2010

We start our analysis by deriving a general integro-differential equation for the slowly varying envelope of the SPP mode in a slot metal–silicon–metal (MSM) plasmonic waveguide. The planar geometry of the waveguide was selected intentionally to allow for an analytic approach. General considerations indicate that the conclusions obtained with our model will hold true for other geometries, specifically for nanowires. Our analysis takes fully into account the vectorial nature of the SPP mode and incorporates all linear and nonlinear effects that may possibly affect its propagation. We examine the impact of different nonlinear effects on the intensity and phase of SPPs, using two approximate analytical solutions of our integro-differential equation in the quasi-continuous-wave (quasi-CW) regime. The results of our analysis are unequivocal: third-order nonlinear effects themselves are too weak to distinctly affect SPPs, but the free-carrier effects initiated by two-photon absorption (TPA) can be used to manipulate light squeezed tightly into the SPP mode.

2. Nonlinear propagation equation

It is convenient to describe the propagation of SPPs along MSM plasmonic waveguides within the frame of the slowly varying envelope approximation (SVEA). As applied to MSM waveguides, the idea of SVEA is to separate the rapid spatial oscillations and steep spatial decay of the SPP field—described by the complex-valued propagation constant $\beta(\omega)$—from its much more slow variation due to the nonlinear effects in silicon. The electric and magnetic field vectors $\mathbf{E}(x,z,t)$ and $\mathbf{H}(x,z,t)$ of the SPP mode are thus represented in the form [28–30]

$$\mathbf{E}(x,z,t) \approx \sqrt{\frac{2}{\mathscr{N}}}A(z,t)\,\mathbf{E}_0(x,\omega)\exp[i(\beta z-\omega t)]+\text{c.c.}, \tag{1a}$$

$$\mathbf{H}(x,z,t) \approx \sqrt{\frac{2}{\mathscr{N}}}A(z,t)\,\mathbf{H}_0(x,\omega)\exp[i(\beta z-\omega t)]+\text{c.c.}, \tag{1b}$$

where $A(z,t)$ is the temporal envelope, $\mathbf{E}_0(x,\omega)$ and $\mathbf{H}_0(x,\omega)$ describe the lateral profile of the SPP mode (unperturbed by the nonlinear effects) at the carrier frequency ω, and $\mathscr{N}$ is a normalization constant. From here onwards, we consider a slot MSM waveguide that is infinite in the y direction and assume that SPPs propagate along its z axis (see Fig. 1). Nevertheless, as will be evident from the following discussion, the conclusions we reach are also valid for MSM nanowires.

It can be readily verified using Eq. (1) that, if we set

$$\mathscr{N}=\frac{1}{2}\int_{-\infty}^{+\infty}\mathbf{e}_z\,[\mathbf{E}_0(x,\omega)\times\mathbf{H}_0^*(x,\omega)]\,\mathrm{d}x+\text{c.c.}, \tag{2}$$

where $\mathbf{e}_z$ is the unit vector in the z direction and an asterisk denotes complex conjugation, then the SPP-mode power per unit width of the plasmonic waveguide (in the y direction) has the form

$$P(z,t)=|A(z,t)|^2\exp(-z/L_{\text{SPP}}),$$

where $L_{\text{SPP}}=(2\,\text{Im}\beta)^{-1}$ is the propagation length of SPPs. Even though, formally, there is ambiguity in the corresponding intensity, $I(z,t)=P(z,t)/\mathscr{D}$, due to an extension of the mode field to infinity in the x direction, the tight confinement of SPPs within the silicon layer makes the effective mode thickness $\mathscr{D}$ approximately equal to the layer thickness d. Mathematically, $\mathscr{D}$ is given by

$$\mathscr{D}=\frac{1}{Q}\left(\int_{-\infty}^{+\infty}|\mathbf{E}_0|^2\,\mathrm{d}x\right)^2,\quad Q=\int_{-\infty}^{+\infty}|\mathbf{E}_0|^4\,\mathrm{d}x, \tag{3}$$

#136997 - $15.00 USD Received 21 Oct 2010; revised 13 Dec 2010; accepted 17 Dec 2010; published 22 Dec 2010

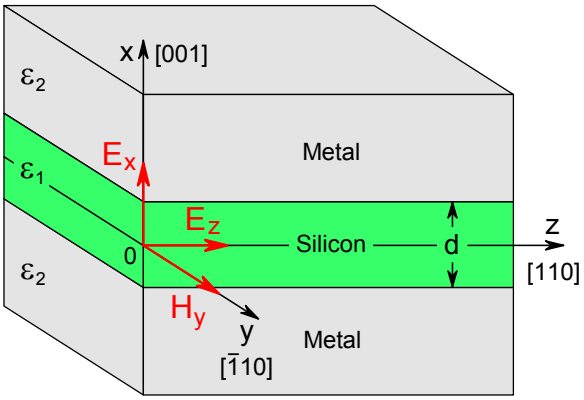

Fig. 1. Geometry of a metal–silicon–metal plasmonic waveguide and electromagnetic field components of the TM SPP mode. Two metallic regions of permittivity ε_2 are separated by a silicon layer of thickness d and permittivity ε_1.

a form naturally arising during derivation of the propagation equation. With this definition, we can apply the same propagation equation for both the MSM and SOI waveguides.

The slot MSM waveguide in Fig. 1 supports only antisymmetric, transverse-magnetic (TM) SPP modes of the form $\mathbf{E}_0 = \{E_x, 0, E_z\}$ and $\mathbf{H}_0 = \{0, H_y, 0\}$. The spatial profile of these modes is given by [31–33]

$$E_x(x,\omega) = \begin{cases} \cos(k_1 x), & |x| < d/2, \\ \cos(k_1 d/2)(\varepsilon_1/\varepsilon_2)\exp[ik_2(|x| - d/2)], & |x| > d/2, \end{cases} \tag{4a}$$

$$E_z(x,\omega) = \frac{k_1}{i\beta} \times \begin{cases} \sin(k_1 x), & |x| \le d/2, \\ \sin(k_1 d/2)\,\mathrm{sign}(x)\exp[ik_2(|x| - d/2)], & |x| \ge d/2, \end{cases} \tag{4b}$$

and $H_y(x,\omega) = Y_j(\omega)E_x(x,\omega)$. Here, $Y_j(\omega) = \varepsilon_0\varepsilon_j\omega/\beta(\omega)$, $k_j = (\varepsilon_j k^2 - \beta^2)^{1/2}$ for $(j = 1,2)$, $k = \omega/c$, and c is the speed of light in vacuum.

The propagation constant β is found from the SPPs' dispersion relation [16]

$$\tanh\left[\frac{ik_1(\omega)\,d}{2}\right] = \frac{\varepsilon_1(\omega)}{\varepsilon_2(\omega)}\frac{k_2(\omega)}{k_1(\omega)}, \tag{5}$$

where we assume $\varepsilon_1(\omega)$ to be real and $\varepsilon_2(\omega)$ to be complex. In the case of ultrathin MSM waveguides with $d \ll |k_1|^{-1}$, Eq. (5) leads to the following explicit form of β:

$$\beta(\omega,d) \approx \frac{1}{d}\left\{\varepsilon_2(kd)^2 + \left[\varepsilon_1/\varepsilon_2 - \sqrt{(\varepsilon_1/\varepsilon_2)^2 + (\varepsilon_1 - \varepsilon_2)(kd)^2}\right]^2\right\}^{1/2}.$$

As an example, the relative error in $|\beta(\omega,d)|$ calculated using this formula at the wavelength of 1.55 μm is below 1.5% for a silver–silicon–silver (Ag/Si/Ag) waveguide with $d \le 50$ nm. A simple analysis of the function $\beta(\omega,d)$ in the limit $d \to 0$ reveals that, in contrast to SOI waveguides where β tends to $\sqrt{\varepsilon_2}\,k$, in MSM waveguides it diverges like $\beta \sim -(2/d)(\varepsilon_1/\varepsilon_2)$. As a consequence of this limiting behavior, $L_{\mathrm{SPP}} \sim d|\varepsilon_2|^2/(4\varepsilon_1 \mathrm{Im}\,\varepsilon_2)$, i.e., the propagation length of SPPs tends to zero in ultrathin waveguides. This feature clearly forces a compromise between strong localization of the field energy and its guiding over reasonable distances.

Our derivation of the propagation equation for $A(z,t)$ closely follows that detailed in Ref. [28] and is not reproduced here. The major difference of the plasmonic problem from optical propagation through SOI waveguides is associated with the decay of SPPs. This decay is taken into

#136997 - $15.00 USD Received 21 Oct 2010; revised 13 Dec 2010; accepted 17 Dec 2010; published 22 Dec 2010

account by employing the equality (see Appendix A)

$$i(\beta+\beta^*)|E_x|^2+E_x\frac{\mathrm{d}E_z^*}{\mathrm{d}x}-E_x^*\frac{\mathrm{d}E_z}{\mathrm{d}x}=i\omega\mu_0(\mathbf{E}_0\times\mathbf{H}_0^*+\mathbf{E}_0^*\times\mathbf{H}_0)\,\mathbf{e}_z, \tag{6}$$

instead of Eq. (A6) in Ref. [28]. The resulting equations for the slowly varying envelope of the fundamental SPP mode and the density N of TPA-generated free carriers are found to be:

$$\frac{\partial A}{\partial z}+\sum_{n=1}^{\infty}i^{n-1}\frac{\beta_n}{n!}\frac{\partial^n A}{\partial t^n}=i\gamma\frac{1+ir}{1+i\varpi}|A|^2A-\frac{\mathscr{B}}{1+i\varpi}\left(\frac{\sigma_\alpha}{2}+ik\sigma_n\right)NA, \tag{7a}$$

$$\frac{\partial N}{\partial t}=-\frac{N}{\tau_{\mathrm{eff}}}+\frac{\hat{\beta}_{\mathrm{TPA}}}{2\hbar\omega\mathscr{D}d}|A|^4, \tag{7b}$$

where $\beta_n=\mathrm{d}^n\beta/\mathrm{d}\omega^n$ is the nth order dispersion parameter.

Other parameters appearing in the preceding two equations are defined as

$$\gamma=\frac{kn_2\eta}{\mathscr{D}}\left(\frac{n_0k\Gamma}{\mathrm{Re}\beta}\right)^2,\quad r=\frac{\beta_{\mathrm{TPA}}}{2kn_2},\quad \mathscr{B}=\frac{\varepsilon_0n_0c}{\mathscr{N}}\int_{-d/2}^{+d/2}|\mathbf{E}_0|^2\,\mathrm{d}x,\quad \Gamma=\frac{\mathrm{Re}\beta}{\mu_0\omega\mathscr{N}}\int_{-\infty}^{+\infty}|\mathbf{E}_0|^2\,\mathrm{d}x,$$

$$\eta=\frac{1}{Q}\sum_{\kappa\lambda\mu\nu}\int_{-d/2}^{+d/2}\mathscr{E}_{\kappa\lambda\mu\nu}E_\kappa^*E_\lambda E_\mu^*E_\nu\,\mathrm{d}x,\quad \hat{\beta}_{\mathrm{TPA}}=\beta_{\mathrm{TPA}}\frac{\eta}{1+\varpi^2}\left(\frac{n_0k\Gamma}{\mathrm{Re}\beta}\right)^2.$$

Here, τ_{eff} is the effective free-carrier lifetime, $n_2=6\times10^{-5}$ cm^2/GW is the nonlinear Kerr parameter, $n_0=3.484$, $\beta_{\mathrm{TPA}}=0.5$ cm/GW, $\sigma_\alpha=1.45\times10^{-21}$ m^2, and $\sigma_n=5.3\times10^{-27}$ m^3 [34–36]. The parameters $\Gamma\geq1$ and $0<\eta<1$ are, respectively, the longitudinal enhancement factor (LEF) and the nonlinear overlap factor (NOF) introduced in Ref. [28]. They show how the nonlinear effects in silicon are enhanced due to the presence of the longitudinal electric field and weakened because SPPs reside partially inside the metal. Using Eq. (6) it is easy to show that, in order for Γ to be close to unity, both the longitudinal electric field and its transverse variation should be small. The fourth-rank tensor $\mathscr{E}_{\kappa\lambda\mu\nu}$ appearing in η characterizes the anisotropy of the Kerr effect and TPA, which depends on the orientation of the principal axes in silicon [37]. The factor $\mathscr{B}>0$ is responsible for enhancement of the free-carrier effects due to confinement of the electric field within the semiconductor layer.

Notice that we do not include in Eq. (7a) the term accounting for linear absorption, since this type of loss is automatically included by the imaginary part of the propagation constant. Except for this term, the fundamental difference between Eqs. (7a) and (7b) and the analogous equations for SOI waveguides [34, 38, 39] lies in the presence of the new parameter

$$\varpi=\frac{\mathrm{Im}\beta}{\mu_0\omega\mathscr{N}}\int_{-\infty}^{+\infty}|E_x|^2\,\mathrm{d}x,$$

which owes its existence to the decay of SPPs along the MSM waveguide. We refer to this parameter as the plasmonic attenuation factor (PAF). The PAF is seen not only to reduce the efficiency of different nonlinear effects, but also to affect their phase. As a result of this influence, for instance, FCA can change the refractive index of the silicon layer, while FCD can affect the intensity of the SPP mode. It should be also noted that various dispersion parameters in Eq. (7a) are complex-valued.

Using the spatial mode profiles given in Eq. (4), we analytically calculate the effective mode thickness $\mathscr{D}$ and other factors (η, Γ, and $\mathscr{B}$) that affect the SPP propagation (see Appendix B

#136997 - $15.00 USD Received 21 Oct 2010; revised 13 Dec 2010; accepted 17 Dec 2010; published 22 Dec 2010

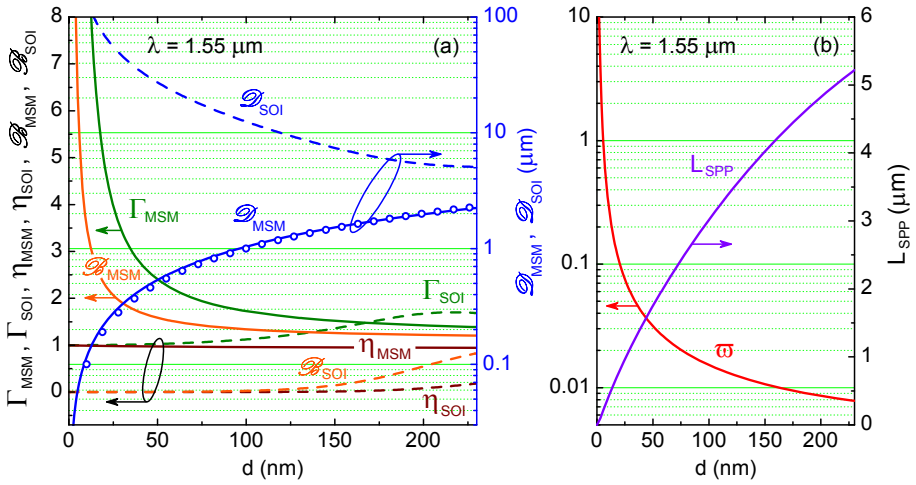

Fig. 2. (a) Parameters Γ, η, $\mathscr{B}$, and $\mathscr{D}$ for the fundamental mode as functions of silicon layer thickness d in MSM (Ag/Si/Ag) and SOI waveguides; circles correspond to $\mathscr{D} = d$. (b) Plasmonic attenuation factor ϖ and SPP propagation length L_{SPP} for the same Ag/Si/Ag waveguide.

for details). Figure 2(a) shows how these parameters vary with the thickness of the MSM waveguide (Ag/Si/Ag) at the telecommunication wavelength $\lambda = 1.55$ μm. We assume that the waveguide is fabricated as shown in Fig. 1 and use the dielectric function of silver from Ref. [40]. For comparison, dashed curves show the same parameters calculated for a single-mode SOI waveguide. It is seen that the factors $\mathscr{B}_{\mathrm{MSM}}$ and Γ_{MSM} diverge as d approaches zero, while η_{MSM} weakly depends on d and tends to unity in this limit; this behavior reflects the increasing confinement of SPPs within the silicon layer. On the other hand, the inability of SOI waveguides to tightly confine optical mode when d is below 200 nm, results in $\mathscr{B}_{\mathrm{SOI}} \to 0$, $\eta_{\mathrm{SOI}} \to 0$ and $\Gamma_{\mathrm{SOI}} \to 1$. Hence, as was expected, the nonlinear effects in an MSM plasmonic waveguide become much more pronounced compared with a SOI waveguide as the waveguides' cross sections decrease. Because the same parameters affect different third-order effects, this conclusion covers all of them, including stimulated Raman scattering (SRS), even though it is neglected in our model.

In Fig. 2(b), we plot the PAF for the same Ag/Si/Ag plasmonic waveguide as a function of its thickness. This factor grows monotonously with decreasing d and becomes proportional to Γ when d tends to zero. For $\lambda = 1.55$ μm, PAF exceed 0.1 and starts affecting the phase of SPPs in waveguides thinner than 20 nm. Meanwhile, the intensity of SPPs is affected in thicker waveguides with $\varpi \gtrsim 0.01$, as will be seen later.

3. Efficiency of nonlinear effects in MSM plasmonic waveguides

In this section we analyze the evolution of a SPP by solving Eq. (7), and estimate quantitatively the magnitude of nonlinear changes in its intensity and phase expected for realistic MSM waveguides.

3.1. Simplified propagation equation

Equation (7) holds for broad range of experimental conditions and can be used to simulate propagation of the TM SPPs over arbitrary distances along an MSM waveguide. In practice, however, it is inefficient to use waveguides that are vastly longer than the propagation length of

#136997 - $15.00 USD Received 21 Oct 2010; revised 13 Dec 2010; accepted 17 Dec 2010; published 22 Dec 2010

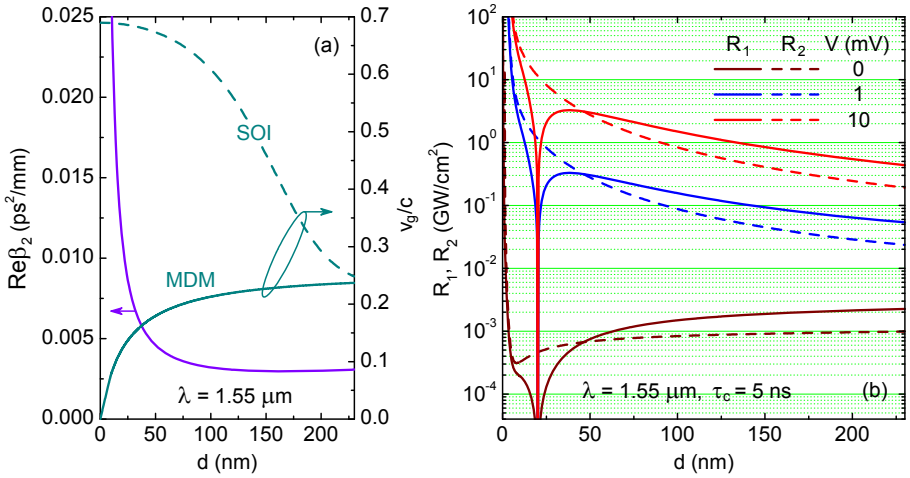

Fig. 3. (a) Group velocity $v_g = (\mathrm{Re}\beta_1)^{-1}$ and dispersion parameter $\mathrm{Re}(\beta_2)$ as a function of the silicon-layer thickness in an MSM plasmonic waveguide; dashed curve shows the group velocity in an SOI waveguide. (b) Ratios $R_1 = |\beta_{\mathrm{eff}}|/(\zeta_r \mathscr{D})$ and $R_2 = \gamma_{\mathrm{eff}}/(|\zeta_i|\mathscr{D})$ as functions of waveguide thickness d for $\tau_{\mathrm{eff}} = 5$ ns, 50 ps, and 5 ps. Other parameters are the same as in Fig. 2.

SPPs. Since this length is typically less than 10 μm [see Fig. 2(b)], dispersive effects of second and higher orders have little impact on the SPP [27]. To illustrate this point, we plot in Fig. 3(a) the real part of group-velocity dispersion parameter β_2, which determines the dispersion length L_D of optical pulses. As can be found using these data, the dispersion length of a 100-fs pulse in a 25-nm-long MSM waveguide exceeds 1 mm, i.e., it comprises of more than 1000 propagation lengths. A further examination shows that this ratio between L_D and L_{SPP} holds approximately for shorter waveguides as well.

By neglecting the dispersion terms in Eq. (7), we can write it in the following compact integro-differential form [38]:

$$\frac{1}{A}\frac{\partial A}{\partial z} = -\left(\frac{\beta_{\mathrm{eff}}}{2} - i\gamma_{\mathrm{eff}}\right)|A|^2 - \left(\frac{\zeta_r}{2} + i\zeta_i\right)\int_0^\infty |A(z,\tau-\tau_{\mathrm{eff}}q)|^4 \exp(-q)\,\mathrm{d}q, \qquad (8)$$

where the four parameters defined as

$$\beta_{\mathrm{eff}} = 2\gamma\frac{r-\varpi}{1+\varpi^2},\ \gamma_{\mathrm{eff}} = \gamma\frac{1+\varpi r}{1+\varpi^2},\ \zeta_r = \frac{\mathscr{B}\hat{\beta}_{\mathrm{TPA}}\tau_{\mathrm{eff}}}{2\hbar\omega\mathscr{D}d}\frac{\sigma_\alpha + 2k\sigma_n\varpi}{1+\varpi^2},\ \zeta_i = \frac{2k\sigma_n - \sigma_\alpha\varpi}{\sigma_\alpha + 2k\sigma_n\varpi}\frac{\zeta_r}{2},$$

are responsible for the TPA, Kerr effect, FCA, and FCD, respectively. The retarded time, $\tau = t - \beta_1 z$ in Eq. (8) is not purely real due to the small imaginary part of β_1; this part is, however, insignificant for even 100-fs pulses and can be safely neglected. Interestingly, β_{eff} and ζ_i can change their sign and become negative in thin MSM waveguides. If this were to take place, TPA will result in amplification of SPPs, and FCD will increase the refractive index of silicon (just as the Kerr effect does). Unfortunately, as will become evident from the following discussion, these unusual properties are unlikely to be utilized in practice.

Similar to the situation in SOI waveguides, the parameters ζ_r and ζ_i are proportional to the effective free-carrier lifetime. By varying τ_{eff}, we can shift the relative importance of the third-order nonlinear effects and free-carrier effects. The effective free-carrier lifetime can be substantially reduced by removing carriers from the optical mode region through the application

#136997 - $15.00 USD Received 21 Oct 2010; revised 13 Dec 2010; accepted 17 Dec 2010; published 22 Dec 2010

of a static electric field. If V is the external voltage applied to the metallic parts of the MSM waveguide, then $\tau_{\rm eff}$ is given by the relation

$$\tau_{\rm eff}^{-1} = \tau_c^{-1} + 2\mu V/d^2,$$

where $\mu \approx 1000\ {\rm cm}^2/({\rm V}\cdot{\rm s})$ [39] is the carrier mobility and τ_c is the free-carrier lifetime in the absence of rejection. For example, by applying a voltage of 10 mV to a 100-nm-thick MSM waveguide, we reduce $\tau_{\rm eff}$ from ns-range to 5 ps, while staying well below the breakdown field of $\approx 3\times 10^5\ {\rm V/cm}$ for silicon.

3.2. Propagation of SPPs in the quasi-CW regime

Consider an optical pulse of width $T_0 \gg \tau_{\rm eff}$ (quasi-CW pulse), so that we may set $A(z,\tau - \tau_{\rm eff}q) \approx A(z,\tau)$ in Eq. (8). The resulting equation has a well known analytical solution [41] of the form $A(z,\tau) = \sqrt{I(z,\tau)}\exp[i\varphi(z,\tau)]$. In order to separately estimate the efficiency of different nonlinear effects in MSM plasmonic waveguides, we use explicit solutions of this equation in two specific cases; (i) when TPA and the Kerr effect dominate over FCA and FCD, the solution is given by

$$I_{\rm K}(z,\tau) = \frac{I_0(\tau)}{1+\beta_{\rm eff}I_0(\tau)\mathscr{D}z}, \quad \varphi_{\rm K}(z,\tau) = \frac{\gamma_{\rm eff}}{\beta_{\rm eff}}\ln\left|1+\beta_{\rm eff}I_0(\tau)\mathscr{D}z\right|; \tag{9}$$

(ii) in the opposite limit, where FCA and FCD dominate over TPA and the Kerr effect, the solution has the form

$$I_{\rm FC}(z,\tau) = \frac{I_0(\tau)}{\sqrt{1+2\zeta_r I_0^2(\tau)\mathscr{D}^2 z}}, \quad \varphi_{\rm FC}(z,\tau) = -\frac{\zeta_i}{2\zeta_r}\ln\left|1+2\zeta_r I_0^2(\tau)\mathscr{D}^2 z\right|. \tag{10}$$

Here, $I_0(\tau)$ is the temporal profile of the input pulse used to excite the SPP inside the MSM waveguide. It is easy to see that solution (9) is applicable when

$$\max\left[I_{\rm K}(z,\tau)\right] \ll \min\left(\frac{|\beta_{\rm eff}|}{\zeta_r\mathscr{D}}, \frac{\gamma_{\rm eff}}{|\zeta_i|\mathscr{D}}\right),$$

while the solution (10) is valid as long as

$$I_{\rm FC}(z,\tau) \gg \max\left(\frac{|\beta_{\rm eff}|}{\zeta_r\mathscr{D}}, \frac{\gamma_{\rm eff}}{|\zeta_i|\mathscr{D}}\right).$$

The two ratios involved in the above inequalities are plotted in Fig. 3(b) for three values of the dc voltage. It is seen that, if $\tau_{\rm eff} = 5$ ns ($V = 0$), free-carrier effects are by far much stronger than the Kerr effect and TPA for all intensities of practical interest. As $\tau_{\rm eff}$ is reduced to 50 ps ($V = 1$ mV), TPA and the Kerr effect start to dominate for $I_{\rm K} \sim 1\ {\rm GW/cm}^2$ in MSM waveguides thinner than 15 nm. To make FCA and FCD negligible as compared to the third-order effects in thicker waveguides, $\tau_{\rm eff} = 5$ ps ($V = 10$ mV) is required.

Of primary importance for practical applications is the extent of changes induced by different nonlinear effects in the SPP mode. As we mentioned earlier, the natural characteristic length that should be used to estimate these changes is the propagation length of SPPs. Figure 4 shows the intensity and phase of the quasi-CW SPP, once it covers a distance of $L_{\rm SPP}$ through MSM waveguides of different thicknesses. It was assumed that $\tau_{\rm eff} = 5$ ns, and the free-carrier effects dominate. One can see that the FCD can produce nonlinear phase shifts $\sim \pi$ within a length of only 1–2 μm for a 30-nm-thick MSM waveguide. At the same time, FCA may be

#136997 - $15.00 USD Received 21 Oct 2010; revised 13 Dec 2010; accepted 17 Dec 2010; published 22 Dec 2010

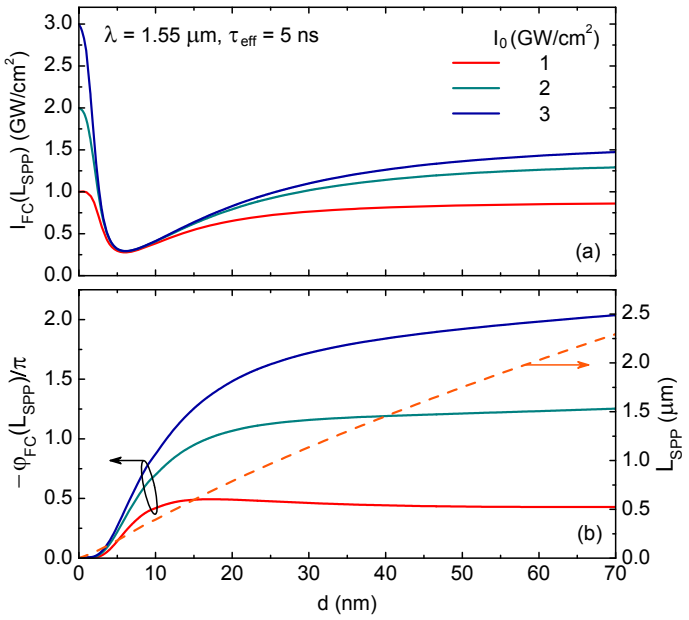

Fig. 4. (a) Intensity and (b) nonlinear phase shift as functions of d for a quasi-CW SPP excited inside a plasmonic waveguide (Ag/Si/Ag) when free-carrier effects dominate over TPA and the Kerr effect; dashed curve shows propagation length of SPPs. Simulation parameters are the same as in Fig. 2.

rather moderate, if the pulse intensity is not very high. These results imply that the free-carrier effects can be successfully employed to realize all FCA- and FCD-based device functionalities on a nanoscale that have been previously demonstrated on a centimeter scale with the SOI technology. These applications include all-optical switching [41–45], wavelength conversion [46], optical modulation [47, 48], and pulse compression [49].

Similar estimations for the Kerr effect and TPA performed with Eq. (9) show that $\varphi_{\mathrm{K}}(L_{\mathrm{SPP}})/\pi \lesssim 0.005$, and the relative decrease in intensity is below 0.5%, irrespective of the specific values of $I_0 < 10$ GW/cm^2 and $d < 230$ nm. Thus, for making use of the third-order nonlinear effects in silicon for the SPPs, the prediction is rather unfavorable: they are too weak to develop on the length scale of L_{SPP} and unlikely to be employed in practice. It is easy to ascertain the reason behind such a result. In the limit $d \to 0$, the coefficients β_{eff} and γ_{eff} behave like $\propto \Gamma^2$, whereas ζ_r and ζ_i grow much faster—as a product $\mathscr{B}\Gamma^2$ [see Fig. 3(b)]. Physically, this discrepancy is due to different dependance of the free-carrier and third-order nonlinear effects on optical intensity. Since SRS also stems from the third-order susceptibility, it is clear that neither Raman amplification nor lasing are likely to be possible with the silicon-based plasmonic waveguides (despite the fact that SRS coefficient in silicon is much bigger than the TPA coefficient). Of course, one can always introduce gain into silicon layer to compensate for ohmic losses and allow SPPs to build up sufficient gain or phase shift [21–23, 27]. However, in this case, the advantage of strong localization of optical power, conferred by MSM waveguides, will be completely offset by their increased length.

As a closing remark, it is worth noting that the derived equations are quite applicable to MSM waveguides with ultrathin silicon layers ($d \sim 1$ nm), in which the field intensity is extremely high. This situation seems unusual for SOI waveguides, where nonlinear effects produced by strong optical fields significantly perturb the lateral mode profile. In MSM waveguides, the

#136997 - $15.00 USD Received 21 Oct 2010; revised 13 Dec 2010; accepted 17 Dec 2010; published 22 Dec 2010

intensity of the electric field becomes more and more uniform inside the silicon layer, as its thickness decreases. As a consequence, the intensity-dependant nonlinear effects cannot modify the lateral profile of the SPP mode, and the accuracy of the approximations used to derive Eq. (7) improves.

4. Conclusions

We have examined the possibility of building photonic devices by employing the nonlinear optical phenomena in silicon-based plasmonic waveguides. Although, for simplicity and concreteness, we analyzed a slot silver–silicon–silver plasmonic waveguide at $\lambda = 1.55$ μm, our conclusions are valid for other waveguide geometries and wavelengths, and are not specific to silver. Our estimates show that, even though all nonlinear effects are substantially stronger in a metal-silicon-metal (MSM) plasmonic waveguide than in a SOI waveguide of the same thickness, the reduced length of the MSM waveguide makes the Kerr effect, two-photon absorption, and stimulated Raman scattering too inefficient for device applications. Fortunately, the free-carrier effects remain strong enough even in a 10-nm-thick MSM waveguide that is only 500-nm long, and they can dramatically affect the propagation of SPPs. Therefore, it is free-carrier absorption and free-carrier dispersion that should be used to control light in nano-sized, silicon-based plasmonic waveguides.

Appendix A

Equation (6) is a special case of a more general relation

$$i(\beta+\beta^*)|\tilde{\mathbf{E}}_T|^2+\tilde{\mathbf{E}}_T\nabla_T\tilde{E}_z^*-\tilde{\mathbf{E}}_T^*\nabla_T\tilde{E}_z=i\omega\mu_0(\tilde{\mathbf{E}}\times\tilde{\mathbf{H}}^*+\tilde{\mathbf{E}}^*\times\tilde{\mathbf{H}})\,\mathbf{e}_z, \tag{11}$$

which holds for any solution of the Maxwell's equations of the form

$$\tilde{\mathbf{E}}(\mathbf{r})=\mathbf{E}_0(x,y)\exp(i\beta z),\quad \tilde{\mathbf{H}}(\mathbf{r})=\mathbf{H}_0(x,y)\exp(i\beta z).$$

To prove this relation, we rewrite its right side using the law of induction, $i\omega\mu_0\tilde{\mathbf{H}}=\nabla\times\tilde{\mathbf{E}}$,

$$i\omega\mu_0(\tilde{\mathbf{E}}\times\tilde{\mathbf{H}}^*+\tilde{\mathbf{E}}^*\times\tilde{\mathbf{H}})\,\mathbf{e}_z=\mathbf{e}_z\left[\tilde{\mathbf{E}}^*\times[\nabla\times\tilde{\mathbf{E}}]\right]-\text{c.c.} \tag{12}$$

Employing the vector-triple-product identity and decomposing the electric field into transverse and longitudinal components, we obtain

$$\begin{aligned}\mathbf{e}_z\left[\tilde{\mathbf{E}}^*\times[\nabla\times\tilde{\mathbf{E}}]\right]=\mathbf{e}_z[\nabla(\tilde{\mathbf{E}}^*\tilde{\mathbf{E}})-(\tilde{\mathbf{E}}^*\nabla)\tilde{\mathbf{E}}]&=\tilde{\mathbf{E}}^*\frac{\partial\tilde{\mathbf{E}}}{\partial z}-(\tilde{\mathbf{E}}^*\nabla)E_z\\&=i\beta|\tilde{\mathbf{E}}|^2-(\tilde{\mathbf{E}}_T^*\nabla_T)E_z-i\beta\tilde{E}_z^2=i\beta|\tilde{\mathbf{E}}_T|^2-(\tilde{\mathbf{E}}_T^*\nabla_T)E_z.\end{aligned}$$

Substituting this result in Eq. (12), we arrive at Eq. (11).

#136997 - $15.00 USD Received 21 Oct 2010; revised 13 Dec 2010; accepted 17 Dec 2010; published 22 Dec 2010

Appendix B

Denoting the real and imaginary parts of k_j as k_j' and k_j'' for $(j=1,2)$ and using Eq. (4), we obtain

$$\mathscr{I}_1 \equiv \int_{-d/2}^{+d/2} |\mathbf{E}_0|^2\,\mathrm{d}x = \Pi_+^{(1)} - \left|\frac{k_1}{\beta}\right|^2 \Pi_-^{(1)}, \quad \Pi_\pm^{(\nu)} = \frac{1}{2}\left[\frac{\sin(\nu k_1' d)}{k_1'} \pm \frac{\sinh(\nu k_1'' d)}{k_1''}\right],$$

$$\int_{-\infty}^{+\infty} |\mathbf{E}_0|^2\,\mathrm{d}x = \mathscr{I}_1 + \frac{1}{k_2''}\left\{\left|\frac{\varepsilon_1}{\varepsilon_2}\cos\left(\frac{k_1 d}{2}\right)\right|^2 + \left|\frac{k_1}{\beta}\sin\left(\frac{k_1 d}{2}\right)\right|^2\right\},$$

$$\int_{-\infty}^{+\infty} |E_x|^2\,\mathrm{d}x = \Pi_+^{(1)} + \frac{1}{k_2''}\left|\frac{\varepsilon_1}{\varepsilon_2}\cos\left(\frac{k_1 d}{2}\right)\right|^2,$$

$$Q = \Lambda_+ + \left|\frac{k_1}{\beta}\right|^4 \Lambda_- - \frac{1}{4}\left|\frac{k_1}{\beta}\right|^2 \Pi_-^{(2)} + \frac{1}{2k_2''}\left\{\left|\frac{\varepsilon_1}{\varepsilon_2}\cos\left(\frac{k_1 d}{2}\right)\right|^2 + \left|\frac{k_1}{\beta}\sin\left(\frac{k_1 d}{2}\right)\right|^2\right\}^2,$$

$$\Lambda_\pm = \frac{d}{4} + \frac{\Pi_+^{(2)}}{8} \pm \frac{1}{2}\,\mathrm{Re}\left[\frac{\sin(k_1 d)}{k_1}\right],$$

and

$$\mathscr{N} = \varepsilon_0\omega\left\{\mathrm{Re}\left(\frac{\varepsilon_1}{\beta}\right)\Pi_+^{(1)} + \mathrm{Re}\left(\frac{\varepsilon_2}{\beta}\right)\frac{1}{k_2''}\left|\frac{\varepsilon_1}{\varepsilon_2}\cos\left(\frac{k_1 d}{2}\right)\right|^2\right\}.$$

Since $E_y = 0$ for the TM SPP mode (see Fig. 1), only the following eight components of the anisotropy tensor contribute to the material polarization [37]:

$$\mathscr{E}_{xxxx} = 1, \quad \mathscr{E}_{zzzz} = \frac{1+\rho}{2}, \quad \mathscr{E}_{xxzz} = \mathscr{E}_{zzxx} = \mathscr{E}_{xzzx} = \mathscr{E}_{zxxz} = \mathscr{E}_{xzxz} = \mathscr{E}_{zxzx} = \frac{\rho}{3},$$

where $\rho \approx 1.27$ in the 1.55-μm region. With these components, we find that

$$\eta Q = \Lambda_+ + \frac{1+\rho}{2}\left|\frac{k_1}{\beta}\right|^4 \Lambda_- - \frac{\rho}{6}\left|\frac{k_1}{\beta}\right|^2 \Pi_-^{(2)} - \frac{2}{3}\rho\left\{\mathrm{Re}\left(\frac{k_1^2}{\beta^2}\right)\left[\frac{d}{4} - \frac{\Pi_+^{(2)}}{8}\right] + \frac{1}{2}\,\mathrm{Im}\left(\frac{k_1^2}{\beta^2}\right)\mathrm{Im}\left[\frac{\sin(k_1 d)}{k_1}\right]\right\}.$$

The same expressions are applicable to SOI waveguides, after the replacement $\sinh(\nu k_1'' d)/k_1'' \to \nu d$.

Acknowledgments

The work of I. D. Rukhlenko, M. Premaratne, and G. P. Agrawal was sponsored by the Australian Research Council (ARC) through its Discovery Grant scheme under grants DP0877232 and DP110100713. The work of G. P. Agrawal was also supported by the NSF Award ECCS-0801772.

#136997 - $15.00 USD Received 21 Oct 2010; revised 13 Dec 2010; accepted 17 Dec 2010; published 22 Dec 2010